Iranian Journal of Pharmaceutical Sciences
2021: 17 (2): 67-86
www.ijps.ir

Original Article

Deciphering the Possible Role of Statins as Antibacterial Agents through Molecular Modelling Approach

Srikanth Jupudi*, Athira TP, Mohammed Afzal Azam

Department of Pharmaceutical Chemistry, JSS College of Pharmacy, JSS Academy of Higher Education & Research, Ooty, Nilgiris, Tamil Nadu, India.

Abstract

The global incidence of resistance to commonly used antibiotics was a challenging public health concern that justifies the urgency in developing novel antibacterial agents. ATP-dependent Mur ligases (MurC, MurD, MurE, and MurF) are validated targets in antibacterial drug design. Drug repurposing or drug repositioning is an alternative strategy in identifying new indications for the currently approved drugs. Statins are currently FDA-approved drugs used to treat hyperlipidemia. The pleiotropic effects of statins, along with their anticipated antibacterial properties, encouraged us to investigate them against MurD ligase of *Escherichia coli* and *Staphylococcus aureus*. The molecular docking and MMGB-SA studies revealed that amongst all selected statins, pravastatin exhibited higher binding affinity with the catalytic residues of *Escherichia coli* (-7.24 kcal/mol and -88.36 kcal/mol) and *Staphylococcus aureus* (-7.47 kcal/mol and -63.75 kcal/mol) MurD ligases. Further, 20 ns MD simulation showed stability and favorable interaction pattern of pravastatin with both enzymes.

Keywords: *Escherichia coli*, MMGB-SA, Molecular dynamics, MurD ligase, Statins, *Staphylococcus aureus*.

Corresponding Authors: Srikanth Jupudi, Department of Pharmaceutical Chemistry, JSS College of Pharmacy, JSS Academy of Higher Education & Research, Ooty, Nilgiris, Tamil Nadu, India
Tel: +91-9393011114
Email: sjphd@jssuni.edu.in
Cite this article as Jupudi S, TP A, Afzal Azam M, Deciphering the Possible Role of Statins as Antibacterial Agents through Molecular Modelling Approach, 2021, 17 (2): 67-86.

1. Introduction

Bacterial resistance to the currently available antibiotics and a global increase in mortality and morbidity has raised a quest to discover novel and effective antibacterial agents. The ATP dependent bacterial cytoplasmic enzymes MurC-MurF are reported to be validated targets and play crucial role in successive addition of L-alanine, D-glutamic acid (D-Glu), meso-diaminopimelic acid (mDAP in Gram-negative bacteria) or L-lysine (in Gram-positive bacteria) and D-alanine-D-alanine to UDP-N-acetylmuramic acid leading to the formation of peptidoglycan precursor UDP N-acetylmuramoyl pentapeptide chain or park nucleotide. Bacterial MurD ligase (UDP-N-acetylmuramoyl-L-Alanine: D-Glutamate ligase), second in the Mur Ligase family, catalyzes the ATP-dependent peptide bond

formation between cytoplasmic intermediate UDP-N-acetyl-muramoyl-L-alanine (UMA) and incoming D-Glutamic acid to give UDP-N-acetylmuramoyl-L-Alanine-D-Glutamate (UMAG) with the release of ADP and phosphate. The 3D-crystal structure of all bacterial MurD liagses consists of three domains. The N-terminal domain is responsible for fixing the UDP moiety of UMA precursor chain, the central domain characterized by Rosmann fold involves in the ATP fixation, while the C-terminal domain is involved in the fixing of the incoming D-Glu. Due to its high specificity for D-amino acids and absence in mammals makes MurD as a promising target for the development of new antibacterial drugs [1, 2]. A 31% and 62% of sequence identity was observed for *Escherichia coli* MurD (*Ec*MurD) with MurD of *Bacillus subtilis* and *Haemophilus influenza*, respectively and low sequence similarity with *Staphylococcus aureus* MurD (*Sa*MurD).

N-acetylmuramic acid as tetrahedral transition-state analogs of *Ec*MurD with low inhibitory activity was discovered, which ultimately led to phosphorylated hydroxyethylamines with enhanced IC_{50} values [3, 4]. Further substituted naphthalene-N-sulfonyl glutamic acids were reported as promising inhibitors with an IC_{50} value in the micromolar range [5, 6]. The findings from the available 3D-crystal structures of flexible and rigid cyclohexane dicarboxylic linked with naphthalene-N-sulfonyl, 5-benzylidenerhodanine, 5-benzylidenethiazolidine-2, 4-diones revealed structural insights into the binding modes of these inhibitors [7, 8, 9]. Structure-based virtual screenings, target-based design ,and de novo structure-based approaches reported D-Glu-based inhibitors possessing 5-benzylidenethiazolidin-4-one scaffold as potent inhibitors of *Ec*MurD with IC_{50s} ranging between 3-7 µM [10]. Further studies evaluated the furan-based benzene-1, 3-dicarboxylic acids as inhibitors against a cascade of Mur ligases (MurC- MurF) [9, 11]. These findings conceded the presence of the D-Glu scaffold as a recognition pattern for binding with the catalytic pocket residues. Our recent structure-based *in silico* high-throughput virtual screening approach identified a virtual hit CACPD2011a-0001827917 with IC_{50} value 7 µM against *Sa*MurD [12].

The bottlenecks in the current antibacterial drug discovery comprise lack of chemical diversity, plummet in the antibiotic pipeline, development of resistance, escalation in drug discovery cost and time, and low incentives in antibacterial R&D. These factors rerouted the scientists away from conventional drug development to a conceptualized strategy called Drug repurposing. Drug repurposing or drug repositioning is an alternative strategy in identifying new indications for the currently approved drugs. Statins, the lipid-lowering drugs that inhibit the 3-hydroxy-3-methylglutaryl coenzyme A (HMG-CoA) reductase, thereby inhibiting the cholesterol synthesis are used to treat hyperlipidemia. There are seven FDA-approved marketed statins: pravastatin, fluvastatin, lovastatin, pitavastatin, atorvastatin, rosuvastatin and simvastatin. The pleiotropic effects of statins

include periodontitis treatment, expression of nitric oxide synthase, restoring endothelial function, antithrombic, immunomodulatory, and anti-inflammatory properties. Along with these, some *in vitro* data suggest that statins are anticipated to have antibacterial properties. This reduces the risk of infections in patients suffering from metabolic diseases like diabetes and also acts as an adjuvant in host-directed therapies [13-23]. The antibacterial studies on statins either alone or in combination with other antimicrobial drugs revealed synergistic action with lower MIC values. This indicated the efficacy of statins towards several bacteria strains [24-31]. Further, it was shown that simvastatin with a lower MIC value is more effective against all types of microorganisms, whereas fluvastatin and pravastatin exhibited low MIC only against *Streptococcus pneumonia*. Other studies showed atorvastatin with significant antibacterial activity against almost all strains of Gram-negative bacteria [32]. Unfortunately, fractional inhibitory concentration index (FICI) data which determines the additive or antagonistic or synergistic effect of other drugs in combination with antimicrobial agents revealed, no statin having synergistic action [32, 33]. However, encouraging results for the usage of statins as antibacterial drugs, the insufficient data concerning the therapeutic concentration of statins without any adverse drug reactions, and tackling resistant pathogenic bacteria are incentives for researchers to expand their studies in this subject.

The resemblance of 3, 5-dihydroxyheptanoic acid side chains (3, 5-DHHA) and hydroxyl lactone moieties of statins with glutamic acid recognition patterns of MurD ligase inhibitors (Figure 1), and also the evinced antibacterial properties of statins intrigued us to study the binding interactions of statins in the active sites of *E. coli* and *S. aureus* MurD as a starting point to repurpose these scaffolds as a platform for the development of antibacterial agents. For validating the proposed hypothesis, we performed molecular docking, molecular dynamics, and MM/GBSA studies to find the interaction pattern of statins in the catalytic pockets of *E. coli* and *S. aureus* MurD ligases.

2. Materials and Methods

2.1. Molecular Docking and Free Energy Calculation Studies

The 2D structures of seven selected statins: fluvastatin, atorvastatin, simvastatin, lovastatin, pitavastatin, pravastatin, rosuvastatin (Figure 2), were downloaded from PubChem in SDF format and prepared using Ligprep (Maestro 12.0, Schrödinger 2019-2, LLC, New York, NY). Ligprep adds hydrogens, assign bond orders, generates low-energy 3D-conformations and possible tautomeric states at physiological pH 7.0 ± 2. The chirality of statins was maintained, and finally, energy minimization was performed with the OPLS3e force field until the RMSD reached 0.01Å. The MurD ligase of *E. coli* (2Y1O.*pdb*, resolution 1.49 Å) was processed using the protocols as described earlier [34], and the homology built of *S. aureus* MurD [35] was used for the present study. The extra-precision (XP) dockings of prepared statins

were performed with Glide without applying any constraints. Based on the glide score and glide energy values, the best-docked poses of statins were selected. The MM/GBSA approach was used to calculate the binding free energies of the selected statins/protein complexes. Prime molecular mechanics generalized born surface area (MM/GBSA) of Schrödinger suite 2019-2 integrates; the VSGB 2.0 energy-based continuum solvent model and OPLS3e force field [36].

2.2. Molecular Dynamics

The binding modes of pravastatin in the active site of *Ec*MurD and modelled *Sa*MurD were investigated by performing 20 ns molecular dynamics (MD) simulations with Desmond software (Schrödinger 2019-2) and OPLS3e force field [36]. The complexes were solvated with explicit TIP4P [37, 38] water and neutralized with seventeen sodium cations. The energy of solvated system was minimized using steepest descent (200 steps) followed by conjugate gradient (1000 steps) until reaching the gradient threshold of 25 kcal/mol/Å. An ensemble of NVT and NPT was maintained, respectively at 300K and 1.00 bar. Multiple time step RESPA integration algorithm was used with time steps of 2, 2, and 6 fs, respectively for bonded, near non-bonded, and far non-bonded interactions. Limited memory Broyden-Fletcher-Goldfarb-Shanno (LBFGS) algorithm with a convergence threshold gradient of 1 kcal/mol/Å was also used for energy minimization. The long-range electrostatic interactions (cut-off radius of 9 Å) and the short-range van der Waals and Coulomb interactions (at a tolerance of $1e^{-09}$) were treated with the Smooth Particle Mesh Ewald method [39]. The data collected for every 100 ps trajectory were analyzed using the simulation interaction diagram in Maestro graphical interface.

3. Results and Discussion

3.1. Molecular Docking and Binding Free Energy (MM/GBSA) Studies

The binding poses of statins unveiled hydrogen bonding, hydrophobic and polar interactions with the active site residues of *Ec*MurD and *Sa*MurD ligases. Glide docking results are presented in Table 1and Table 2. Glide score values for the selected statins in the active site of *Ec*MurD ranges between -3.97 to -7.25 kcal/mol. In the active site of *Ec*MurD, the 3,5-dihydroxy heptanoic acid (3,5-DHHA) moiety of pravastatin, pitavastatin, atorvastatin, fluvastatin, and rosuvastatin occupied the C-terminal domain, while in simvastatin and lovastatin, the 4-hydroxy-6-oxotetrahydro-2H-pyran ring occupied the same domain. All these statins exhibited hydrogen bonding interactions with Lys115, Glu157, Arg186, Lys319, Thr321, Lys348, Ser415, and Phe422 residues. In the *Ec*MurD docked pose of pitavastatin (gscore-7.25 kcal/mol) (Figure 3a) the 3,5-DHHA moiety occupied the N-terminal domain and established four hydrogen-bonding interactions, one each with Leu13, Thr16, and two hydrogen bonds with Arg37. The hydroxyl group present at position three of 3, 5-DHHA established two hydrogen-bonding interactions with the backbone >C=O of Leu13 (-OH···O=C-, 2.12 Å) and the NH of Thr16

(HO···H-N-, 2.67 Å). The carboxylate and carbonyl oxygen atoms of the same moiety established hydrogen bonding interactions with the side chain NH of Arg37 (-C=O···H-N-, 1.64 Å; -C-O^{-}···H-N-, 1.76 Å).

As depicted in Figure 3b, pravastatin (gscore-7.24 kcal/mol) formed substrate (UMAG) specific interactions in the C-terminal domain. It shared a total of six hydrogen bonds with Lys115, His183, Lys319 and Ser415. The oxygen of the hydroxyl group, present at position five of 3, 5-DHHA, formed a hydrogen bond with the side chain OH of Ser415 (HO···H-O-, 2.37 Å). The terminal carbonyl oxygen and OH present at position three of 3, 5-DHHA shared two hydrogen bonds one each with the side NH of Lys319 (>C=O···H-N-, 1.97 Å and HO···HN-, 2.19 Å). His183 formed two hydrogen bonds with the carboxylate oxygen (-C-O^{-}···H-N-, 2.37 Å) of 3, 5-DHHA and the carbonyl oxygen of 2-methylbutanoate moiety (-C(=O)···HN-, 2.63 Å). The carboxylate oxygen (-C(=O)-O^{-}···HN-, 2.78 Å) of 3,5-DHHA also shared one hydrogen bond with the side chain of Lys115. Similar results are also obtained from the gscores of seven statins in the catalytic pocket of *Sa*MurD. Glide score values for the selected statins in the active site of *Sa*MurD ranges between -4.33 to -7.64 kcal/mol. In the docked pose of pitavastatin (Figure 4a) two hydroxyl groups of 3,5-DHHA shared two hydrogen bonds, one each with Thr330 (HO···HO-, 2.12 Å) and Asn331 (HO···H-N-, 2.11 Å). The backbone >C=O and the side chain -NH of Lys328 shared two hydrogen bonds, respectively, with the hydroxyl group (-OH···O=C-, 2.12 Å) present on position five and the carboxylate oxygen (-C(=O)-O^{-}···H-N-, 1.84 Å) of 3,5-DHHA. The NH of Lys19 showed a π-π stacking with the pyridine part of the quinoline ring. It is evident from Fig. 4b that the pravastatin is established in the active site of *Sa*MurD by sharing three hydrogen bonds, one each with Lys19 (HO···HN-, 2.21Å), Ser20 (HO···HN-, 2.57 Å), and Asn78 (-OH···O=C<, 1.79Å) of N-terminal domain. Whereas, hydroxyl group present at position three of 3,5-DHHA formed two hydrogen bonds, one each with the side chain NH of Lys122 (HO···HN-, 2.44Å) and the side chain imidazole ring of His192 (-OH···N<, 2.13 Å). The binding poses of the other five statins are represented as 2D-interaction diagrams in Fig. 5 and Fig. 6.

The comparable MM/GBSA energies of statins (Table 3 and Table 4) indicated that van der Waal energy with higher negative values in both *E. coli* (-63.82 to -61.4 kcal/mol) and *S. aureus* (-46.79 to -29.92 kcal/mol) made a predominant contribution for overall binding free energy. With the energy values of -28.5 to -13.16 kcal/mol for *Ec*MurD and -22.96 to -8.61 kcal/mol for *Sa*MurD the hydrophobic interaction term partially favored the ligand binding. Hydrogen bond interaction terms (-16.48 to -0.46 kcal/mol and -19.92 to 0.62 kcal/mol) made minor contributions to the total binding. In contrast to the docking score, pitavastatin showed poor binding energy values in *E. coli* (-40.63 kcal/mol) and *S. aureus* (-6.90 kcal/mol). High negative ΔG bind values indicate stronger pravastatin binding in

*Ec*MurD (-88.36 kcal/mol) and *Sa*MurD (-63.75 kcal/mol).

3.2. Molecular Dynamics Simulation

In order to get an insight into the binding modes of pravastatin in the catalytic pockets of both *E. coli* and *S. aureus* MurD we performed 20ns MD simulations using the respective docked complexes. During MD simulation of pravastatin/*Ec*MurD complex, a slight conformational deviation of approximately 1.6 Å was observed in the RMSD of Cα (1.43-3.08 Å) and backbone (1.47-3.07 Å) atoms (Figure 7a). The RMSD of Cα (3.08 Å) and backbone (3.07 Å) atoms spiked up to 10.4 ns and then stabilized (Cα- 2.22-2.57 Å and backbone-2.09-2.58 Å) during the rest of the simulation trajectory. The Cα and backbone atoms showed fluctuation within the range 0.5-2.5 Å, indicating the stability of the protein. In contrast, RMSF (Figure 7b) of ligand-bound residues showed minor fluctuations in the range 0.6-1.6 Å. An abrupt pattern in ligand RMSD (Figure 7a) from 2.1 to 5.4 Å suggests higher flexibility of pravastatin, primarily due to low frequent interaction pattern with 3, 5-DHHA chain. As illustrated in Fig. 7c, Arg37 and Gly73 participated in hydrogen bonding interactions with pravastatin, while Pro41, Ile74, Ile139, Phe161, and Lue416 exhibited low-frequency hydrophobic contacts in the catalytic pocket. As represented in Fig. 7d, the hydroxyl group at position six of hexahydronaphthalene formed a strong and a moderate frequency hydrogen bond, respectively with Gly73 (HO···H-N-, 90% of MD) and Ser71 (-OH···O=C(O^-)-, 29% of MD). A low-frequency hydrogen bonding interaction was also observed between the hydroxyl group present at positions five of 3, 5-DHHA, and Leu416 (HO···O=C(O^-)-, 21% of MD). Arg37 shared two moderate hydrogen bonds in the bidentate manner (-C(=O)O^-···H-N- and –(O^-)C=O···H-N-, total 58% of MD) with two oxygen atoms of the terminal carboxylate group. The fifth position hydroxyl group of the same fragment also formed a water-mediated interaction with Lys348. No significant hydrogen bonds were observed between the 2-methyl butanoate chain and the catalytic residues of *Ec*MurD.

The 20ns simulation trajectory of the pravastatin/*Sa*MurD complex revealed the stability of protein Cα and backbone atoms (Figure 8a) with RMSD of 1.65-2.5 Å and 1.65-2.6 Å, respectively. Cα atoms reached a maximum RMSD of 3.5 Å at 15 ns which plummeted to 2.26 Å at the end of the simulation. The Cα and backbone atoms of ligand-bound residues exhibited RMSFs, respectively, in the range 0.53 to 1.58 Å and 0.57-1.50 Å (Figure 8b). During MD simulation of pravastatin/*Sa*MurD complex hydrogen bonding, hydrophobic and extensive water mediated interactions were observed. Ser20, Asn78, Gly80, Lys122, Asn145, Glu166, Ser168, Lys328, and Arg355 formed moderate to stable hydrogen bonds throughout the simulation (Figure 8c). The 20ns molecular dynamics trajectory pose of pravastatin in the catalytic pocket of *Sa*MurD ligase, as illustrated in Fig. 8d, reveals that 3,5-DHHA was anchored in its position by a solid multiple hydrogen-bonding network with the charged

and polar residues Lys122, Lys328, and Arg311. Water bridged interactions with Thr119, Thr123, Asn145, Glu166, Thr330, Arg311, and Asn331 also played a crucial role in stabilizing pravastatin in the active site of *Sa*MurD. Lys122 formed three strong hydrogen bonds with 3, 5-DHHA hydroxyl group present at position three and two carboxylate oxygen atoms during simulation trajectory. The carbonyl oxygen of the carboxylate group formed a weak hydrogen bond with Lys328 (-C(O^-)=O···HN-, 26% of MD). The two oxygen atoms of the carboxylate group interacted with Arg311 (-C(O^-)=O···H-N-; -C(=O)O^-···HN-) by forming two stable hydrogen bonds with 54% and 57% of the total simulation trajectory. The ligand is further stabilized by water-mediated interactions with Thr330, Asn331, Arg311, Glu166, Thr123, Asn145, and Thr119 with carbonyl oxygens of 2-methyl butanoate chain and 3, 5-DHHA chain. Unlike pravastatin/*Ec*MurD, no significant interactions were observed between hexahydronaphthalene ring and catalytic residues of *Sa*MurD.

Pravastatin, of all statins, exhibited higher binding energy against both *Ec*MurD (-88.36 kcal/mol) and modeled *Sa*MurD (-63.75 kcal/mol) ligases. In pravastatin, the Columbic, hydrogen bonding, lipophilic, and Van der Waal energies played as key contributing factors (Tables 3 and 4). When compared with the reference compounds (h and i in Figure 2) as reported earlier, in *Ec*MurD the XP docking pose of inhibitor 7 (Glide gscore: -9.16 kcal/mol; ΔG_{bind}: -122.02 kcal/mol) with IC_{50} 8.2 µM [34] formed stable hydrogen bonds with Thr36, His183, Thr321, Lys348, Ser415 and Phe422 (Figure 9a). The carboxyl oxygen of the glutamic acid chain exhibited crucial hydrogen bonding interactions with conserved residues His183, Thr321, Lys348, Ser415, and Phe422. The carboxyl and hydroxyl oxygen of pravastatin 3, 5-DHHA chain (Figure 3b) retained two interactions with His183 and Ser415, inferring the access of this chain into the glutamic acid recognition site. In *Sa*MurD the compound 5d (Glide gscore: -5.31 kcal/mol; ΔG_{bind}: -85.33 kcal/mol) with IC_{50} 13.37µM [35] formed hydrogen bonds with Lys19, Ser20, His196, Asp426 and Glu432 (Figure 9b). The XP docked pose of pravastatin in the catalytic pocket of *Sa*MurD retained two hydrogen-bonding interactions with Lys19 and Ser20 and also the formation of hydrogen bond with Lys122 and His192 stabilized pravastatin.

From the molecular dynamics studies, the glutamic acid recognition pattern, 3, 5-DHHA chain formed extensive hydrogen bonding and water bridged interactions in *Sa*MurD proving as an essential feature and also interactions formed by the hydroxyl group on hexahydronaphthalene ring also stabilized the ring in the catalytic site of *Ec*MurD (Figure 7d and 8d). The obtained insights signify pravastatin as a starting point in further investigating its role as a potential MurD ligase inhibitor.

4. Conclusion

Drug repurposing is shown as an emerging paradigm to address the bottlenecks in the current antibacterial drug discovery. Statins are approved lipid-lowering drugs in the treatment of heart attacks and strokes. The present *in*

silico investigation was aimed to rationale the antibacterial activity by predicting the molecular interactions of glutamic acid recognition patterns of statins against MurD ligases. The molecular docking, molecular dynamics simulations, and MMGB-SA studies disclosed the stability of pravastatin in the catalytic pocket of MurD ligases by forming a network of hydrogen bonds with C-terminal residues. Also, the observed high binding affinity of pravastatin with MurD ligases further encourages the need to perform experimental work to validate and support these activities of statins.

References

[1] Walsh AW, Falk PJ, Thanassi J, Discotto L, Pucci MJ, Ho HT. Comparison of the D-glutamate-adding enzymes from selected Gram-positive and Gram-negative bacteria. *J. Bacteriol.* (1999) 181 (17): 5395-5401.

[2] El Zoeiby A, Sanschagrin F, Levesque RC. Structure and function of the Mur enzymes: development of novel inhibitors. *Mol. Microbiol.* (2003) 47 (1): 1-12.

[3] Auger G, van Heijenoort J, Blanot D. Synthesis of N-Acetylmuramic acid derivatives as potential inhibitors of the D-glutamic acid-adding enzyme. *J. Prakt. Chem.* (1995) 337 (1): 351-57.

[4] Sova M, Kovac A, Turk S, Hrast M, Blanot D, Gobec S. Phosphorylated hydroxylethyl-amines as novel inhibitors of the bacterial cell wall biosynthesis enzymes MurC to MurF. *Bioorg. Chem.* (2009) 37 (6): 217-22.

[5] Kotnik M, Humljan J, Contreras-Martel C, Oblak M, Kristan K, Herve M, et al. Structural and functional characterization of enantiomeric glutamic acid derivatives as potential transition state analog inhibitors of MurD ligase. *J. Mol. Biol.* (2007) 370 (1): 107-15.

[6] Humljan J, Kotnik J, Contreras-Martel C, Blanot D, Urleb U, Dessen A, et al. Novel naphthalene-N-sulfonyl-D-glutamic acid derivatives as inhibitors of MurD, a key peptidoglycan biosynthesis enzyme. *J. Med. Chem.* (2008) 51 (23): 7486-94.

[7] Tomasic T, Zidar N, Kovac A, Turk S, Simcic M, Blanot D, et al. 5- Benzylidene thiazolidin-4-ones as Multi-target Inhibitors of Bacterial Mur Ligases. *Chem. Med. Chem.* (2010) 5 (2): 286-95.

[8] Tomasic T, Sink R, Zidar N, Fic A, Contreras-Martel C, Dessen A, et al. Dual Inhibitor of MurD and MurE Ligases from Escherichia coli and *Staphylococcus aureus*. *ACS Med. Chem. Lett.* (2012) 3 (8): 626-30.

[9] Perdih A, Kovac A, Wolber G, Blanot D, Gobec S, Solmajer T. Discovery of novel benzene 1, 3-dicarboxylic acid inhibitors of bacterial MurD and MurE ligases by structure-based virtual screening approach. *Bioorg. Med. Chem. Lett.* (2009) 19 (10): 2668-73.

[10] Zidar N, Tomasic T, Sink R, Kovac A, Patin D, Blanot D, et al. New 5-benzylidenethiazolidin-4-one inhibitors of bacterial MurD ligase: design, synthesis, crystal structures, and biological evaluation. *Eur. J. Med. Chem.* (2011) 46 (11): 5512-23.

[11] Perdih A, Hrast M, Pureber K, Barreteau H, Grdadolnik SG, Kocjan D, et al. Furan-based benzene mono- and dicarboxylic acid derivatives as multiple inhibitors of the bacterial Mur ligases (MurC–MurF): experimental and computational characterization. *J. Comput. Aided. Mol. Des.* (2015) 29 (6): 541-60.

[12] Azam MA, Jupudi S. Structure-based virtual screening to identify inhibitors against *Staphylococcus aureus* MurD enzyme. *Struct. Chem.* (2019) 30: 2123-33.

[13] Bellosta S, Via D, Canavesi M, Pfister P, Fumagalli R, Paoletti R, et al. HMG-CoA Reductase Inhibitors Reduce MMP-9 Secretion by Macrophages. *Arterioscler. Thromb. Vasc. Biol.* (1998) 18 (11): 1671-78.

[14] Koh KK, Ahn JY, Jin DK, Han SH, Kim HS, Choi IS, et al. Comparative Effects of Statin and

Fibrate on Nitric Oxide Bioactivity and Matrix Metalloproteinase in Hyperlipidemia. *Int. J. Cardiol.* (2004) 97 (2): 239-44.

[15] Laufs U, La Fata V, Plutzky J, Liao JK. Upregulation of Endothelial Nitric Oxide Synthase by HMG CoA Reductase Inhibitors. *Circulation* (1998) 97 (12): 1129-35.

[16] Liao JK, Laufs U. Pleiotropic Effects of Statins. *Annu. Rev. Pharmacol. Toxicol.* (2005) 45: 89-118.

[17] Endres M, Laufs U, Huang Z, Nakamura T, Huang P, Moskowitz MA, et al. Stroke Protection by 3-Hydroxy-3-Methylglutaryl (HMG)-CoA Reductase Inhibitors Mediated by Endothelial Nitric Oxide Synthase. *Proc. Natl. Acad. Sci.* (1998) 95 (15): 8880-85.

[18] Pickup JC. Inflammation and Activated Innate Immunity in the Pathogenesis of Type 2 Diabetes. *Diabetes Care* (2004) 27 (3): 813-23.

[19] Hennessy E, O Callaghan J, Mooij MJ, Legendre C, Camacho-Vanegas O, Camacho SC, et al. The impact of simvastatin on pulmonary effectors of *Pseudomonas aeruginosa* infection. *PLoS One* (2014) 9: e102200.

[20] Friesen JA, Rodwell VW. The 3-hydroxy-3-methylglutaryl coenzyme-A (HMG-CoA) reductases. *Genome. Biol*. (2004) 5 (11): 248.

[21] Jain MK, Ridker PM. Anti-inflammatory effects of statins: clinical evidence and basic mechanisms. *Nat. Rev. Drug. Discov.* (2005) 4 (12): 977-87.

[22] Guerra-De-Blas PDC, Torres-Gonzalez P, Bobadilla-Del-Valle M , Sada-Ovalle I , Ponce-De-Leon-Garduno A, Sifuentes-Osornio J. Potential Effect of Statins on Mycobacterium tuberculosis Infection. *J. Immunol. Res.* (2018) 2018: 7617023.

[23] Kaminska M, Aliko A, Hellvard A, Marczyk A, Mydel P. Effects of statins on multispecies oral biofilm. *J. Oral. Microbiol.* (2017) 9 (sup1): 1325249.

[24] Graziano TS, Cuzzullin MC, Franco GC, Schwartz-Filho HO, de Andrade ED, Groppo FC et al. Statins and antimicrobial effects: Simvastatin as a potential drug against *Staphylococcus aureus* biofilm. *PloS One.* (2015) 10 (5): e0128098.

[25] Jerwood S, Cohen J. Unexpected antimicrobial effect of statins. *J. Antimicrob. Chemother.* (2008) 61(2): 362-64.

[26] Masadeh M, Mhaidat N, Alzoubi K, Al-azzam S, Alnasser Z. Antibacterial Activity of Statins: A comparative study of atorvastatin, simvastatin, and rosuvastatin. *Ann. Clin. Microbiol. Antimicrob.* (2012) 11: 13.

[27] Parihar SP, Guler R, Khutlang R, Lang DM, Hurdayal R, Mhlanga MM, et al. Statin therapy reduces the Mycobacterium tuberculosis burden in human macrophages and in mice by enhancing autophagy and phagosome maturation. *J. Infect. Dis.* (2014) 209 (5): 754-63.

[28] Thangamani S, Mohammad H, Abushahba MFN, Hamed MI, Sobreira TJP, Hedrick VE, et al. Exploring simvastatin, an antihyperlipidemic drug, as a potential topical antibacterial agent. *Sci. Rep.* (2015) 5: 16407.

[29] Skerry C, Pinn MLO, Bruiners N, Pine R, Gennaro ML, Karakousis PC. Simvastatin increases the *in vivo* activity of the first-line tuberculosis regimen. *J. Antimicrob. Chemother.* (2014) 69 (9): 2453-57.

[30] Lobato LS, Rosa P S, Ferreira J S, Neumann Ada S, da Silva M G, do Nascimento D C, et al. Statins increase rifampin mycobactericidal effect. *Antimicrob. Agents. Chemother.* (2014) 58 (10): 5766-74.

[31] Dutta NK, Bruiners N, Pinn ML, Zimmerman MD, Prideaux B, Dartois V, et al. Statin adjunctive therapy shortens the duration of TB treatment in mice. *J. Antimicrob. Chemother.* (2016) 71(6): 1570-77.

[32] Gupta M, Kumar A. Comparison of Minimum Inhibitory Concentration (MIC) Value of Statin Drugs: A Systematic Review. *Anti-Infective Agents.* (2019) 17 (1): 4-19.

[33] Eljaaly K, Alshehri S. An updated review of interactions of statins with antibacterial and antifungal agents. *J. Transl. Sci.* (2017) 3 (3): 1-4.

[34] Azam MA, Jupudi S. Extra precision docking, free energy calculation and molecular dynamics studies on glutamic acid derivatives as MurD inhibitors. *Comput. Biol. Chem.* (2017) 69: 55-63.

[35] Azam MA, Jupudi S, Saha N, Paul RK. Combining molecular docking and molecular dynamics studies for modelling *Staphylococcus aureus* MurD inhibitory activity. *SAR. QSAR. Environ. Res.* (2019) 30 (1): 1-20.

[36] Roos K, Wu C, Damm W, Reboul M, Stevenson JM, Lu C, et al. OPLS3e: Extending Force Field Coverage for Drug-Like Small Molecules. *J. Chem. Theory. Comput.* (2019) 15 (3): 1863-74.

[37] Jorgensen WJ, Madura JD. Temperature and size dependnce for Monte Carlo simulations of TIP4P water. *Mol. Phys.* (1985) 56 (6): 1381-92

[38] Lawrence CP, Skinner JL. Flexible TIP4P model for moleculardynamics simulation of liquid water. *Chem. Phys. Lett.* (2003) 372 (5-6): 842- 47.

[39] Essmann U, Perera L, Berkowit ML, Darden T, Lee H , Pedersen LG. A smooth particle mesh Ewald method. *J. Chem. Phys.* (1995) 103 (19): 8577-93.

Tables:

Table 1. XP docking results of seven selected statins in the catalytic pocket of *Ec*MurD (2Y1O.*pdb*).

Statins	[a]G_{score}	[b]G_{vdw}	[c]G_{coul}	[d]G_{emodel}	Residues forming hydrogen bonds
pravastatin	-7.24	-25.71	-13.45	-53.51	Lys115, His183, Lys319, Ser415
lovastatin	-3.97	-28.26	-9.734	-51.01	Lys115, Glu157, His183, Lys319, Lys348
simvaststin	-4.81	-34.71	-4.06	-47.90	Lys319, Thr321, Phe422
atrovaststin	-6.81	-35.86	-12.06	-82.23	Glu157, Lys319
pitavastatin	-7.25	-30.23	-11.67	-56.6	Leu13, Thr16, Arg37
fluvastatin	-6.38	-30.14	-10.25	-56.19	His183, Lys319
rosuvastatin	-6.63	-32.22	-14.55	-62.01	Ser71, Arg186, Lys348

[a]Glide score, [b]Glide van der Waals energy, [c]Glide Coulomb energy, [d]Glide model energy.

Table 2. XP-docking results of seven selected statins in the catalytic pocket of modeled SaMurD ligase.

Name of Statin	[a]G_{score}	[b]G_{vdw}	[c]G_{coul}	[d]G_{emodel}	Hydrogen bonding residues
pravastatin	-7.47	-29.91	-14.75	-53.28	Lys19, Ser20, Asn78, Lys122, His192
lovastatin	-4.33	-36.82	-3.28	-51.00	Asn78
simuvaststin	-4.75	-29.18	-4.19	-39.28	His192, Asn331
atrovaststin	-6.17	-37.79	-16.31	-75.21	Lys122, His192, Glu166, Lys328
pitavastatin	-7.64	-29.54	-11.68	-55.51	Thr330, Asn331, Lys328
fluvastatin	-5.27	-29.55	-8.40	-52.10	Lys328
rosuvastatin	-5.77	-29.26	-17.37	-55.91	Asn78, Ser169

[a]Glide score, [b]Glide van der Waals energy, [c]Glide Coulomb energy, [d]Glide model energy.

Table 3. Energy contributions of binding free energy (MM/GBSA) (kcal/mol) of seven selected statins/*Ec*MurD complex (2Y1O.*pdb*).

Name of Statin	[a]ΔG_{bind}	[b]ΔG_{Coul}	[c]ΔG_{Hbond}	[d]ΔG_{Lipo}	[e]ΔG_{vdW}
pravastatin	-88.36	-33.55	-16.48	-28.5	-63.82
lovastatin	-13.55	-16.19	-0.57	-13.16	-42.85
simuvaststin	-30.65	-2.99	-0.46	-17.51	-51.03
atrovaststin	-30.07	79.76	-2.6	-21	-58.01
pitavastatin	-40.63	-11.63	-7.31	-24.94	-45.45
fluvastatin	-37.76	20.76	-5.71	-20.35	-61.4
rosuvastatin	-25.63	66.48	-9.09	-13.8	-51.53

[a]free energy of binding; [b]coulomb energy; [c]hydrogen bonding energy; [d]hydrophobic energy (nonpolar contribution estimated by solvent accessible surface area); evan der Waals energy.

Table 4. Energy contributions of binding free energy (MM/GBSA) (kcal/mol) of seven selected statins/modeled *Sa*MurD complex.

Name of Statin	[a]ΔG_{bind}	[b]ΔG_{Coul}	[c]ΔG_{Hbond}	[d]ΔG_{Lipo}	[e]ΔG_{vdW}
pravastatin	-63.75	-38.68	-19.92	-17.16	-46.79
lovastatin	-41.25	-48.27	0.62	-18.42	-29.15
simvaststin	-40.5	-22.77	-0.64	-17.87	-29.92
atrovaststin	-44.76	34.34	-1.75	-22.96	-25.58
pitavastatin	-6.90	54.47	-0.72	-8.61	-21.61
fluvastatin	-16.22	29.78	-2.02	-12.89	-20.35
rosuvastatin	-37.5	35.42	-8.19	-17.23	-24.7

[a]Free energy of binding; [b]Coulomb energy; [c]hydrogen bonding energy; [d]hydrophobic energy (nonpolar contribution estimated by solvent accessible surface area); [e]van der Waals energy.

Figures:

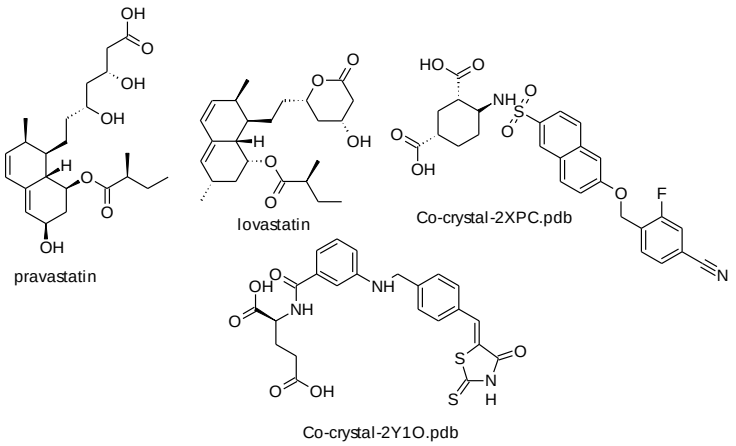

Figure 1. Representation of scaffold similarity in selected statins and Co-crystal structures of MurD ligase.

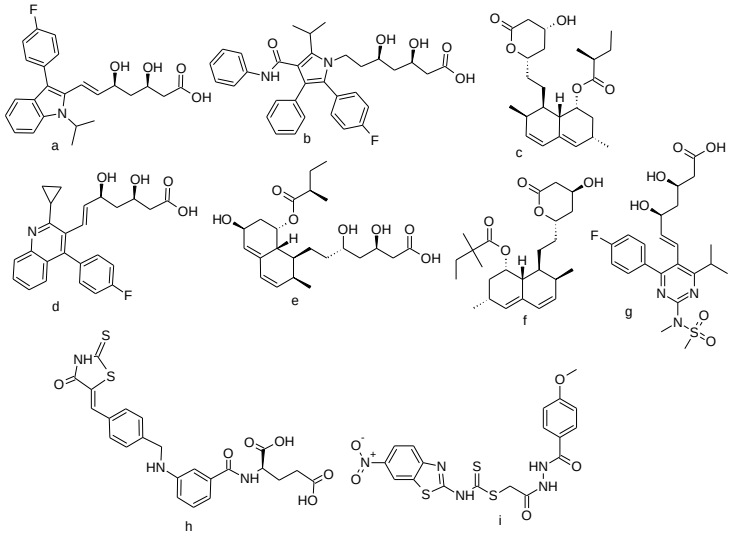

Figure 2. Chemical structures of selected statins (a) fluvastatin (b) atorvastatin (c) lovastatin (d) pitavastatin (e) pravastatin (f) simvastatin (g) rosuvastatin (h) inhibitor 7 (i) compound 5d.

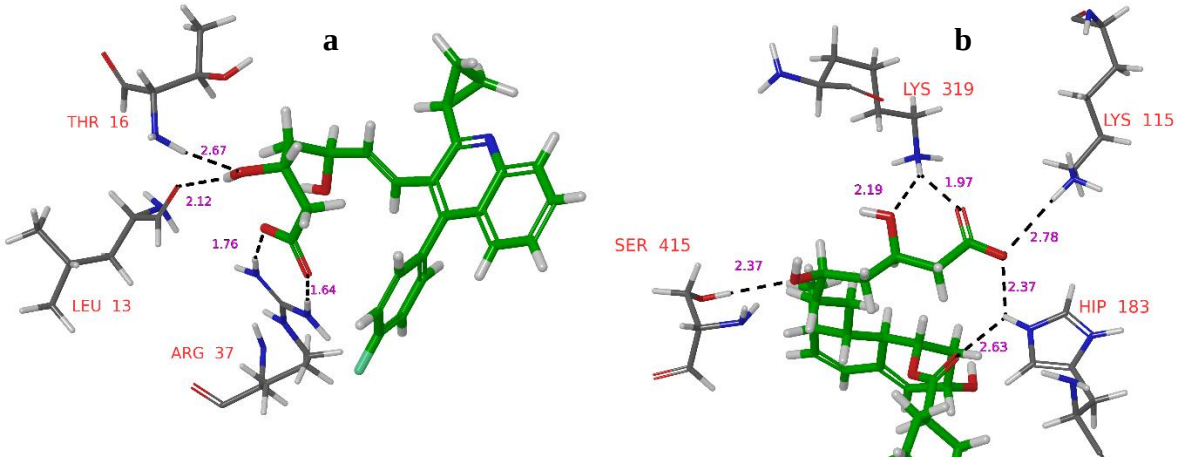

Figure 3. XP-docked poses of top scored statins (a) pitavastatin and (b) pravastatin in the catalytic pocket of *Ec*MurD.

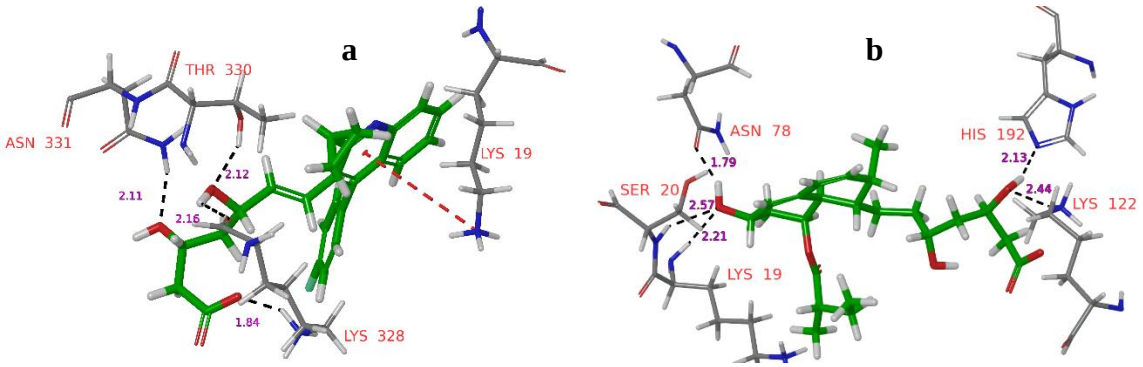

Figure 4. XP docked poses of top scored statins (a) pitavastatin and (b) pravastatin in the catalytic pocket of modeled *Sa*MurD ligase.

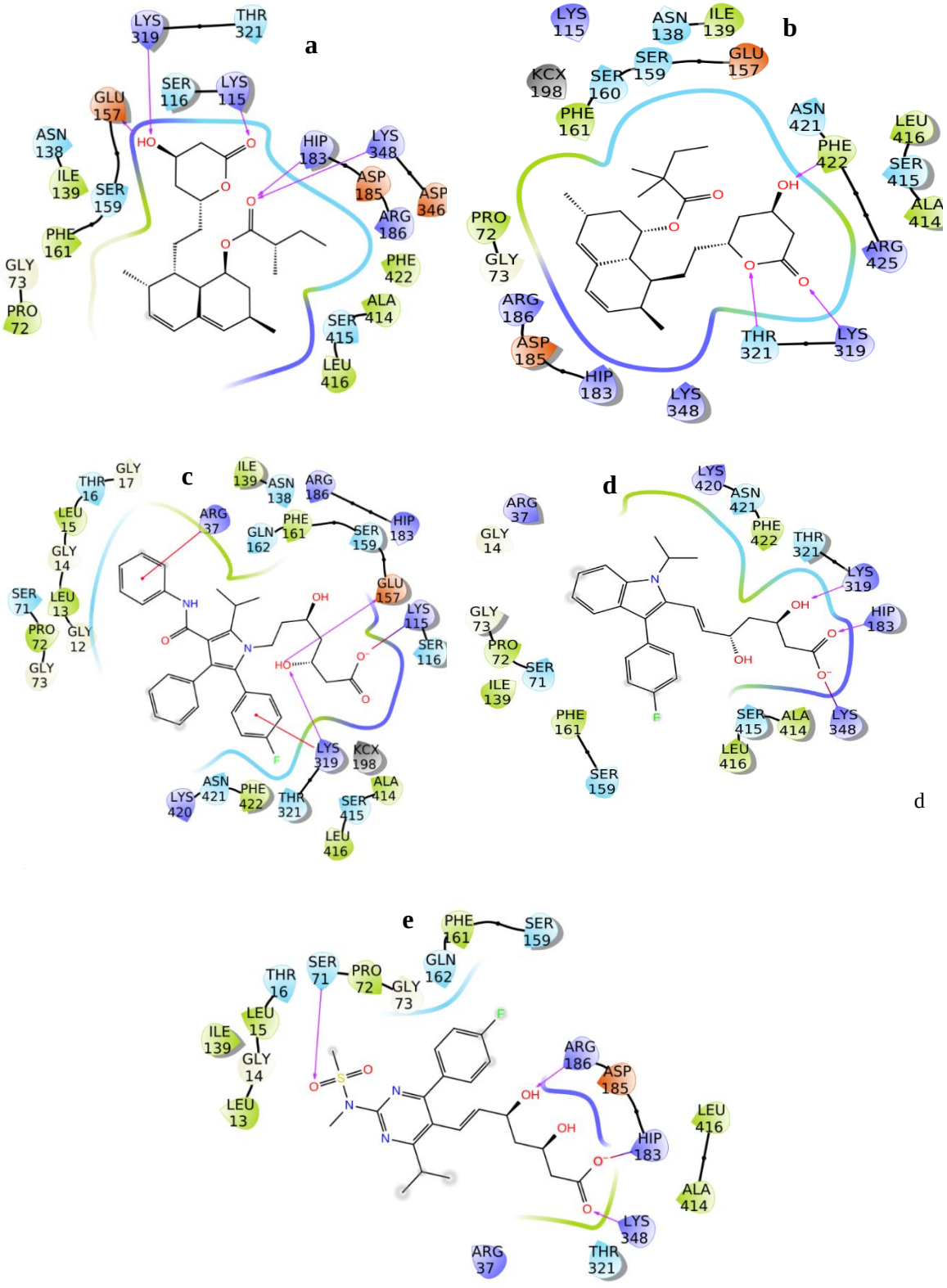

Figure 5. Binding poses of statins in the catalytic pocket of *Ec*MurD ligase (a) lovastatin (b) simvastatin (c) atrovastatin (d) fluvastatin and (e) rosuvastatin.

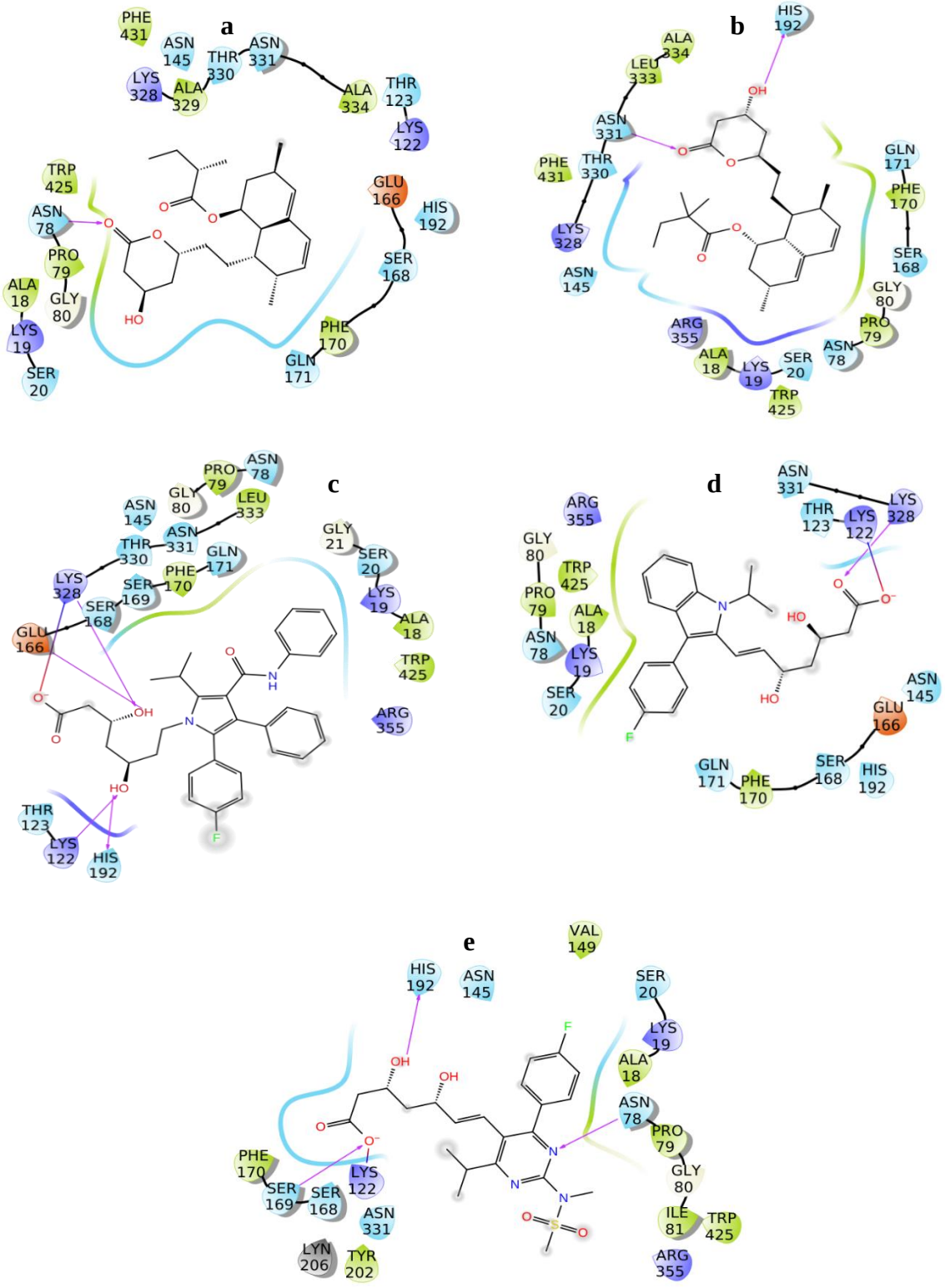

Figure 6. Binding poses of statins in the catalytic pocket of homology built *Sa*MurD ligase (a) lovastatin (b) simvastatin (c) atrovastatin (d) fluvastatin and (e) rosuvastatin

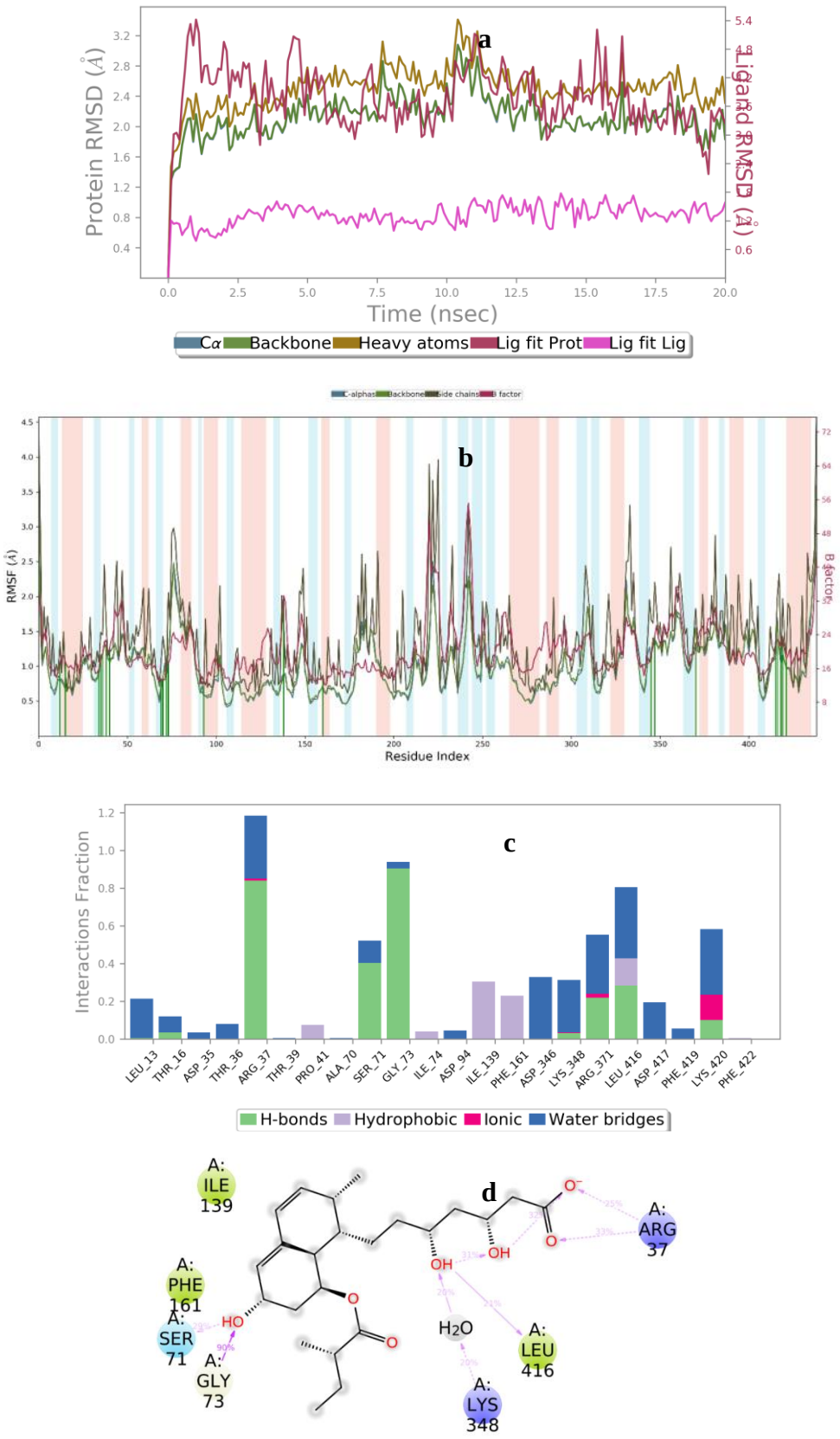

Figure 7. (a) RMSD plot of 20 ns MD simulated pravastatin/*Ec*MurD complex (b) RMSF plot of 20 ns MD simulated pravastatin/*Ec*MurD complex (c) interaction fraction diagram of pravastatin showing different types of contacts over the course of 20 ns trajectory (d) 2D-interaction diagram of pravastatin in complex with *Ec*MurD over 20 ns simulation trajectory.

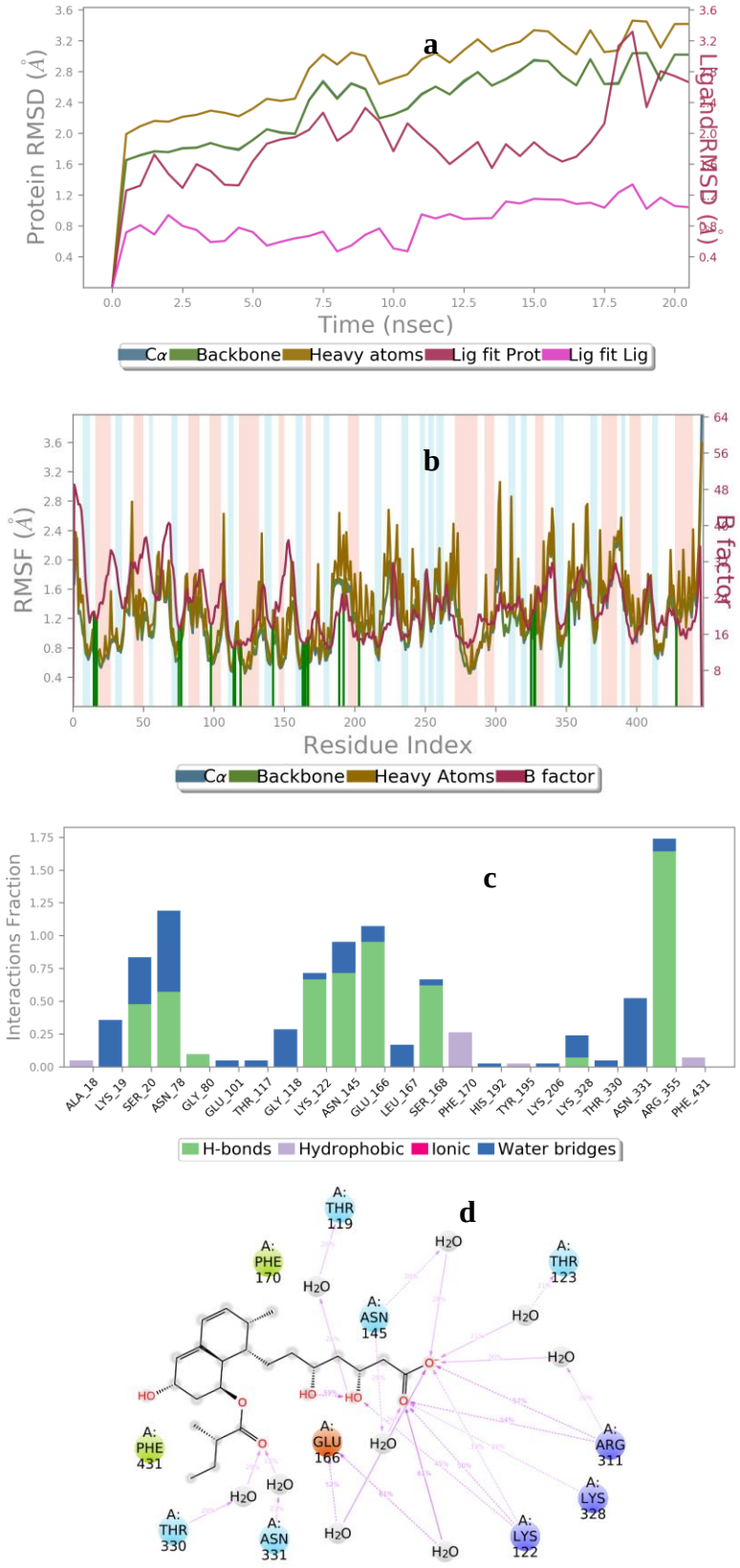

Figure 8. (a) RMSD plot of MD simulated pravastatin/*Sa*MurD complex (b) RMSF plot of MD simulated pravastatin/*Sa*MurD complex (c) interaction fraction diagram of pravastatin/*Sa*MurD complex showing different types of contacts over the course of 20 ns trajectory (d) 2D-interaction diagram of pravastatin/*Sa*MurD complex over 20 ns simulation trajectory.

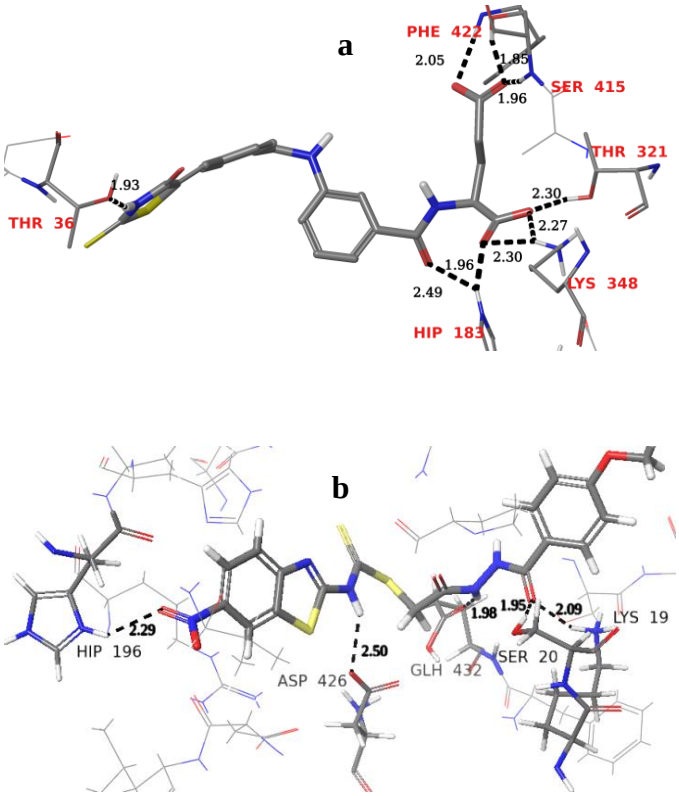

Figure 9. (a) XP docked pose of inhibitor 7 (IC_{50}: 8.2 µM) (b) XP docked pose of compound 5d (IC_{50}: 13.37 µM).

ONLINE SUBMISSION

www.ijps.ir